Numerical and experimental investigation on the forward osmosis (FO) process for the operational conditions and spacer configuration optimization in microalgae dewatering

Haitao Wen[a,b,d], Jie Wang[a,*], Huu Hao Ngo[c,*], Hongwei Zhang[a], Ruzhen Bai[a], Hui Jia[a], Xinbo Zhang[a,d]

[a] *State Key Laboratory of Separation Membranes and Membrane Processes, Tiangong University, Tianjin 300387, China*

[b] *School of Material Science and Engineering, Tiangong University, Tianjin 300387, China*

[c] *Centre for Technology in Water and Wastewater, School of C ivil and Environmental Engineering, University of Technology Sydney, Sydney, NSW 2007, Australia*

[d] *School of Environmental and Municipal Engineering, Tianjin Chengjian University, Tianjin 300384, China*

ABSTRACT

Microalgae (Scenedesmus obliquus) dewatering using forward osmosis membrane has received considerable attention for its possible application in biofuel generation. To investigate the filtration performance by analyzing permeate water flux, five different velocities (0.23 m/s, 0.31 m/s, 0.40 m/s, 0.55 m/s, 0.66 m/s) were selected in a bench-scale experiments. The results showed that the optimal flux was with 0.55 m/s velocity. Moreover, the same velocities (0.23 m/s, 0.31 m/s, 0.40 m/s, 0.55 m/s, 0.66 m/s) and three various spacer positions (0.3 mm, 1 mm and 2 mm away from the membrane) were simulated employing the computational fluid dynamics (CFD) approach. The results showed that the pressure and velocity distribution were affected by the velocities at the module inlet and the spacer configuration. And the 0.55 m/s velocity was confirmed, while the CFD revealed that the velocity distribution was relatively uniform and exerted a higher pressure on the membrane, and 0.55 m/s velocity agreed with the experiment in optimal operation. As for the spacer configurations, they were evenly distributed in the channel and the optimum structures occurred when the spacers were 1 mm away from the membrane. The spacer is beneficial for alleviating external concentration polarization (ECP) during osmosis process.

Keywords: Microalgae dewatering; forward osmosis; computational fluid dynamics; hydraulics condition optimization; external concentration polarization

1. Introduction

Microalgae technology is widely used in food, nutrition, aquatic products, environmental protection, energy, agriculture, industry, etc. And the cost of algae harvesting, cell drying and oil extraction, accounted for 50% of the production cost [1]. The bottleneck of algae water separation restricts the application of microalgae in the fields of sewage nitrogen uptake and advanced treatment large-scale cultivation and energy [2].

Recently, forward osmosis (FO) technology for microalgae pretreatment to further dewatering process has drawn great attention due to its potential low energy consumption, its ability to reject a high level of contaminants, and its being subject to much less membrane fouling [3-5]. The processes of dewatering, usually achieved by centrifugation, flocculation, sedimentation, pressure-driven membrane processes or the combinations of these processes, have a number of disadvantages, such as, high consumption of energy, algal cells breakage, high susceptibility to fouling, and negative effect on biomass quality [6, 7]. For example, Landels *et al.* [8] concentrated on electrocoagulation flotation (ECF), and the efficient, rapid and scalable dewatering of microalgal cultures to yield 13% algal biomass load was ideal for direct downstream processing by hydrothermal liquefaction. Yusra et al. [9] used air-sparging to perform ultrafiltration on microalgae dewatering; the results showed that the gas-sparging could inhibit the formation of microalgae filter cake layer and improve the recovery of permeation flux and biomass. However, these physical or chemical operations are either cost-effective or susceptible to irreversible fouling [10]. Different from those conventional methods, especially pressure-driven membrane processes, FO process, a semipermeable membrane, is placed between a microalgal solution of low concentration (0.1-0.2g dry wt/l) and a draw solution (DS) of high concentration. This can be achieved by driving water through a membrane

under a differential osmotic pressure [11-13]. However, the concentration polarization (CP) phenomenon does occur, accompanied by the separation process, and cause a severe flux decline during the FO process [14-17]. This phenomenon can be further classified as: internal concentration polarization (ICP) in the membrane support layer, and external concentration polarization (ECP) on the membrane surface layer [18, 19].The ECP originating from the solute of feed solution accumulates on the active layer and the draw solution concentration is commonly diluted by the permeating water[20, 21]. It is the barrier that reduces the effective osmosis pressure differential and subsequently the water flux of the process, especially in the low velocity and without spacers [22, 24]. Therefore, it is necessary to determine the hydrodynamic conditions of the membrane surface and optimize the module channel's hydraulic conditions to reduce the influence of ECP [25, 26]. Further research on hydrodynamic characteristics (e.g., spacer design) has been conducted, for example, Liu et al. [27] investigated spacer impacts caused by the velocity field, and proposed that the boundary layer at membrane surface may be disturbed by turbulence and the bulk solution absorb the solute which diffused back from the layer.

The theoretical method of computational fluid dynamics (CFD), as a powerful method, seeks to predict and investigate fluid flow, mass transfer, heat transfer, and other related phenomena [28-31]. Currently, CFD was assisted in the design and associated with running repeated experiments [32, 33]. To investigate the velocity field for a channel with a permeate flow through a wall, Hansen *et al.* [34] established a spectral element method to solve the Navier-Stokes equations, indicating that mass transfer would increase between neighboring filaments due to shedding of vortices. Consequently, the best mass transfer at certain values of filament spacing/channel height ratio was evident [35, 36]. Cao *et al.*[37], evaluating the

velocity profile of the spacer-filled channel by utilizing the CFD simulation method, confirmed that the presence of spacer would cause eddy activity on the membrane surface to promote mass transfer and reduce fouling, while plausibly improving local shear stress. Abdelbaky and El-Refaee [38] reported a spacer channels incorporated in membrane modules for reverse osmosis applications, in which the feed spacer functioned to promote turbulence, improve mass transfer and reduce concentration polarization.

Many CFD simulation studies indicated the relationship between hydraulic configuration and permeation efficiency [39, 40]. This line of research tried to numerically and experimentally optimize the hydraulic conditions on the membrane, and examined the characteristics of flow field under configurations with different flow velocities and spacers in the osmosis process.

To do numerical analysis, forward membrane module has been designed by using 3D CFD simulation, in which liquid velocity and pressure distribution have been taken into consideration [21, 41]. In these studies, to investigate the filtration performance of microalgae dewatering by analyzing permeate water flux，five velocities (0.23 m/s, 0.31 m/s, 0.40 m/s, 0.55 m/s, 0.66 m/s) were selected in lab-scale experiments, then the same velocities and spacer positions (0.3 mm, 1 mm and 2 mm away from the membrane) between the membrane and channel were selected for further study. In addition, the piezo film sensor was employed in the experimental investigation to verify the obtained simulation results.

2. Materials and methods

2.1. Microalgae cultivation and FS/DS preparation

Scenedesmus obliquus (Shanghai Guangyu Biological Technology Co., Ltd.) was chosen

as model microalgal species, due to its frequent application in biofuels production and wastewater treatment [42]. The BG11 medium was used to pre-culture Scenedesmus obliquus, the culture temperature was 25℃, the light intensity was 3000-4000 lx, and the light-dark time ratio was 12h : 12h. The algae suspensions were continuously stirred at room temperature (25±1°C) by injecting air at a rate of 60 l/h.

In the microalgae dewatering experiment with the FO system, 500 ml of Scenedesmus obliquus solution (0.1 g/l) and 200 ml of 1 M NaCl (AR, Tianjin Sinopharm Chemical Reagent, China) were used for FS and DS, respectively. Both FS and DS used deionized water (DI) (Milli-Qgard AZ MingChe® Integral, Merck Millipore, China) and the AL-DS mode (active layer facing draw solution) was adopted.

2.2. Bench scale test system

In the first part of the experiment, to investigate permeate flux during the FO process with an active surface area of approximately 14 cm^2, bench-scale tests were conducted (Figure 1). Two tubing pumps (WT600-2J-YZ1515X, Longer, China) were applied to inject the feed and draw solutions into the channel simultaneously at the different rotating rates of feed and draw solutions to investigate permeate flux difference on the FO membrane.

A commercially available CTA-FO membrane (SeaPack Crew Emergency Desalination Pouch, HTI, USA) was used in this study. Two flow meters LZB-6 were used to monitor the flow rate at both lines of DS and FS in the system. A conductivity meter (HI98197, HANNA, USA) was used to record both conductivity and temperature of the FS. An electronic analytical balance (ME2002T, METTLER TOLEDO, China) was used to measure the weight change of DS and determine the permeate flux at same time.

Five different velocities (0.23 m/s, 0.31 m/s, 0.40 m/s, 0.55 m/s, 0.66 m/s) were selected

to investigate the filtration performance of microalgae dewatering by analyzing permeate water flux. The water flux (l/m^2 ·h) was determined by the following Eq. (1).

$$Jw=\frac{\Delta m}{\rho A t} \qquad (1)$$

where Δm is the measured weight interval for the water that permeates from the FS to the DS (g), ρ is the density of water (g/cm^3), A is the effective membrane surface area (m^2), and t is duration of the experiment (h). The DS weight change was monitored at 5 min intervals by using the ME2002T balance.

2.3. FO membrane module

In the second part of the experiment, the FO membrane module had symmetrical channels that allow separate circulation of FS & DS and it was made from custom-made flat organic glass. The rectangular channel was 7 cm × 2 cm × 0.3 cm in size. The inlet diameter was designed to be 0.4 cm. The membrane was sandwiched between two organic glass plates by using a silicon gasket and six stainless steel screws. The effective membrane area was the same as the first part of the experiment in this module. Furthermore, the CTA FO membrane was placed under the spacers in the feed channel, and the spacer gap was determined by thickness of the silicon gasket.

2.4. Simulation experimental setup

The AL-FS orientation was adopted in FO performance experiments. A piezo film of rectangle area (11 mm × 15 mm in size) was attached to the central section of the membrane surface. The FS and DS were prepared by dissolving analytical grade NaCl (Tianjin Guangfu Fine Chemical Research Institute, China) in pure water or deionized (DI) water (Milli-Qgard AZ MingChe® Integral, Merck Millipore, China). The draw solutions consisted of five concentrations (32 g/l, 50 g/l, 70 g/l, 100 g/l, 117 g/l) while the FS was 5 g/l NaCl resembling

the concentration of brackish water (BW).

The same method was adopted to establish the experimental setup, as shown in Figure 1. And a magnetic stirring apparatus RCT was used to mix the FS and adjust its temperature. An ME2002T scale was used to measure the weight change of draw solution and determine the permeate flux at the same time. Voltage acquisition system used a voltmeter, one end of the voltmeter connected with the piezoelectric film to achieve the output voltage, the other end connected with the computer to obtain real-time count.

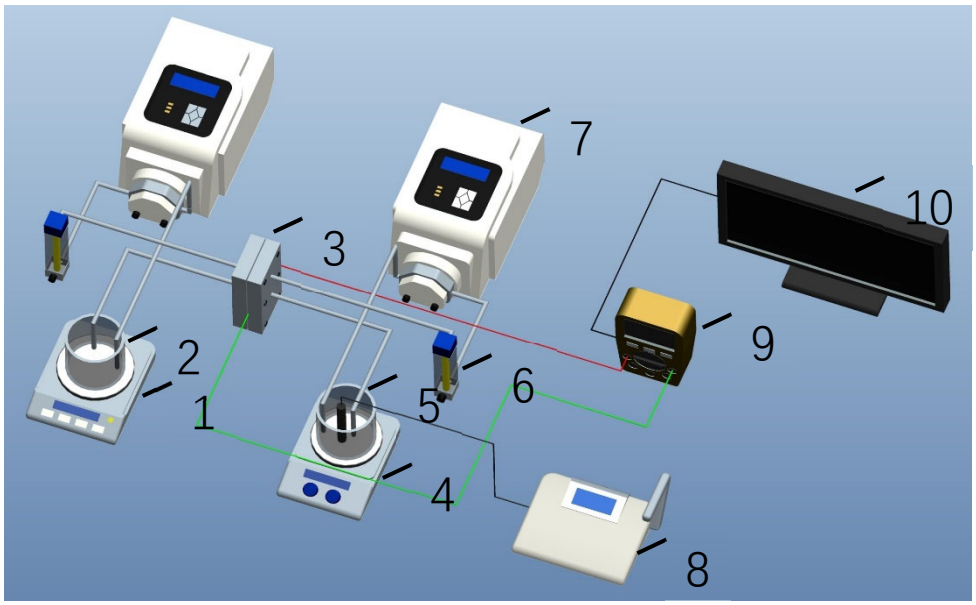

Fig. 1. Schematic diagram for FO experimental setup: 1, electronic balance; 2, draw solution; 3, FO membrane module; 4, magnetic stirring apparatus; 5, feed solution; 6, flow meters; 7, peristaltic pump; 8, conductivity meter; 9, voltage acquisition system; 10, computer.

2.5. Piezo film

Commercially metallized piezo film sheets (11 mm×15mm in size) from MEAS (United States) were used in the second experiment. The upper and lower surfaces of the PVDF film were covered with a thin silver electrode layer, and the conductive silver glue from Capiton Sci-Technology Company was coated with the silver electrode layer to lead the wire from the electrode layer. The silver ink was used for electrode materials of PVDF thick films in the

metallization stage. 28 um thick films were chosen for this analysis. The pressure on the surface of forward membrane was measured by piezoelectric PVDF sensors. The piezoelectric film was attached to the surface of the film for testing, as shown in Fig. 2. PVDF film parameters are shown in Table 1. The operating theory of PVDF film elements was employed that when force is applied to compress or bend the film, PVDF will generate an external charge that is called piezoelectric effect [43], which can be glued to the surface of the electrode to generate electrical signals, i.e. the signal output by the universal meter. The pressure can be calculated by Eq. (2):

$$X = V_0 = g_{3n} X_n t \quad (2)$$

Where g_{3n} is the piezoelectric coefficient, Xn is the stress added in the relative direction, t is piezoelectric film thickness, and n is 3 in our study due to the electrode positions (top, mid, bottom) on the film [44].

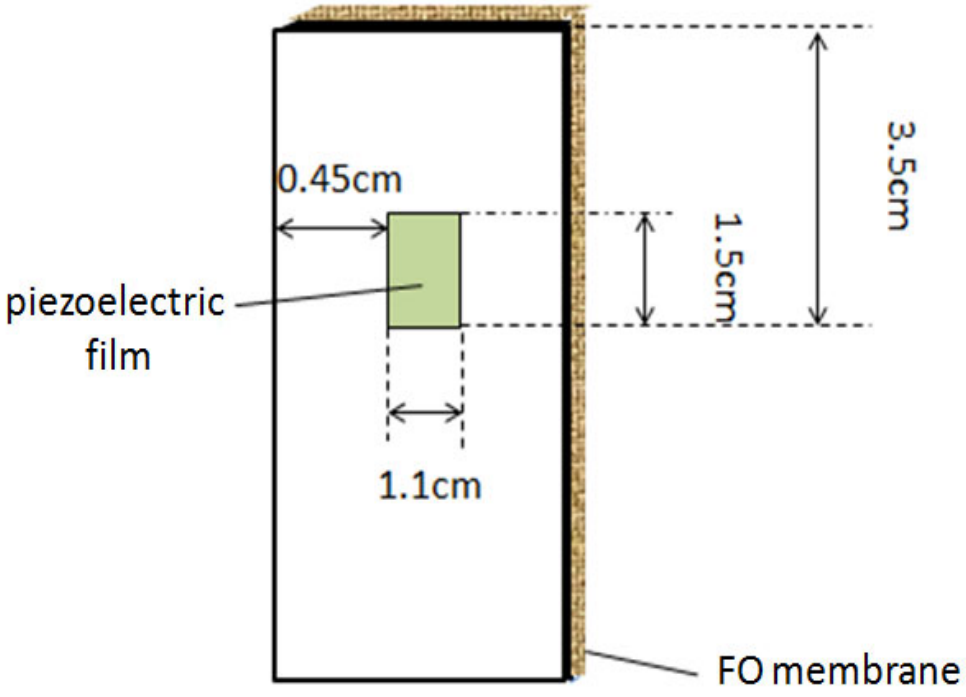

Fig.2. The position of PVDF piezoelectric film on the membrane surface.

Table 1

The parameters of PVDF piezoelectric film.

Parameters	Range
Operating Temperature	-40℃ to 80℃
Piezoelectric constant	-33×10^{-2} C/N
Film thickness	28 μ m
Capacitance	380PF/cm^2@1kHz
Maximum operating voltage	150V/mil(V/ μ m), DC, @25℃

2.6. CFD model and simulations

To examine the hydrodynamic conditions, single-phase flow was used in three-dimensional (3D) simulations to the membrane surface. It was assumed that the fluid is Newtonian, incompressible, and isothermal turbulent, and has constant physical properties under steady-state conditions [1, 45-46]. The governing equations for modeling fluid flow in a steady-state system are the conservation of continuity and momentum equations listed below [47].

(i) Continuity equation

$$\nabla(\rho\vec{v}) = 0 \tag{3}$$

(ii) Momentum equation

$$\nabla(\rho\vec{v}\vec{v}) = -\nabla P + \nabla(\bar{\tau}) + \rho g \tag{4}$$

Where ρ is density (kg/m3), $\vec{v}$ is velocity (m/s), $\bar{\tau}$ is stress tensor (Pa), P is pressure (Pa), τ is surface shear stress (Pa), and g is the gravitational force (N).

In this work, a geometric 3d block module with 15 spacers distributed throughout the length of the chamber was investigated, which was simulated with approximately 390w, 313w and 372w cooper cells with different spacer positions (0.3 mm, 1 mm, 2 mm away from the membrane). A fine mesh was generated because of the importance of flow around the membrane surface and spacers in this region. The model included inlet and outlet tubes with diameters of 4 mm and lengths of 3 mm. To model the flow, combining the SIMPLE pressure-

velocity and segregated solution method, the governing equations were established, and were discretized into a whole volume in the one-order scheme. The standard $k-\varepsilon$ was used to model the turbulent flow behavior [48, 49].

Five analysis surfaces along the gallery were set up at an interval of 10 mm and recorded as Y = 0.01 m, 0.02 m, 0.03 m, 0.04 m, 0.05 m respectively. The flow fields on each analytical surface were investigated for different inlet velocities (0.23 m/s, 0.31 m/s, 0.40 m/s, 0.55 m/s, 0.66 m/s). Fig.3 presents membrane module model and the velocity analysis' location on membrane surface.

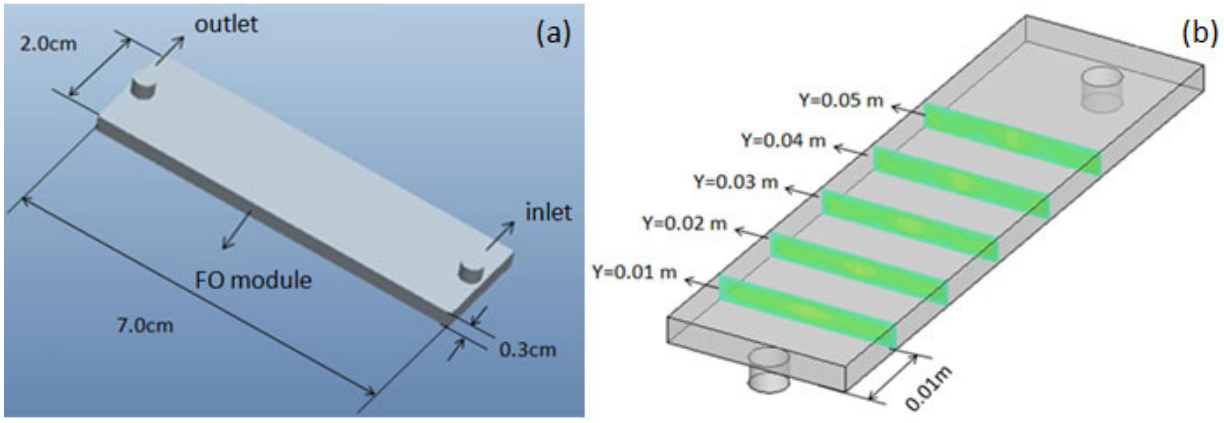

Fig. 3. Membrane module model and the velocity analysis' location on the membrane surface. (a) Membrane module model (b) the velocity analysis' location.

3. Results and discussion

3.1 Effect of different Feed velocities on FO performance

Fig. 4 shows the membrane flux trends in the 6-hour bench-scale experiment under given velocities. As shown in all the cases, the reaction time increased while water flux declined. This decline is attributed to: (1) the loss of osmotic driving force of the whole FO membrane, due to the dilution in the draw solution and (2) membrane fouling [50]. From 0.23m/s to 0.55m/s, the feed velocities was positively related to the value of water flux with a given concentration of draw solution. However, the water flux showed lower value at the velocity of 0.66m/s than at

0.55m/s, but still higher than at other velocities. Thus, 0.55m/s velocity exhibited a much greater water flux, compared with the others during the whole FO process. This observation coincides with the previous study [51]. As the inlet velocities directly change in water flux, to better understand the character of membrane fouling under microalgae dewatering process, the effect of hydraulics conditions in FO process should be investigated.

Fig. 4. FO tests with different inlet velocities under the same DS concentration (1.0 M NaCl): (a) Different Water flux with the DS cross-flow velocity constant at 0.40 m/s; (b) The value of

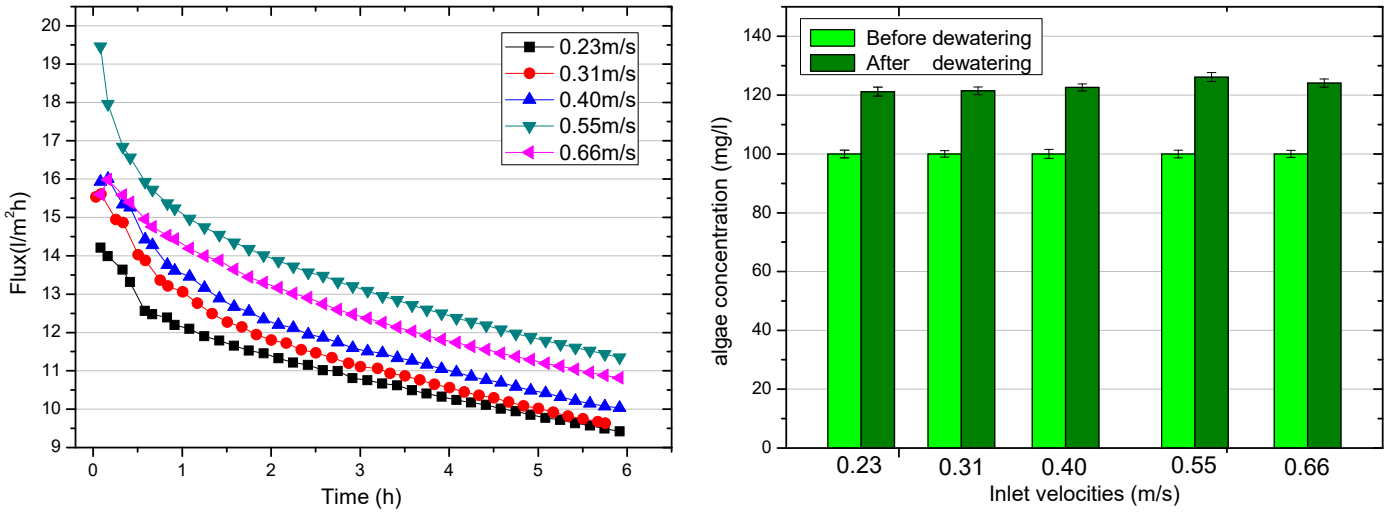

algae concentration with a 14 cm^2 FO membrane under different inlet velocities.

3.2. Impact of operational conditions

Five flow rates ranging from 150 ml/min to 400 ml/min (corresponding to velocities of 0.2–0.7 m/s at the module inlet) were simulated in this study. And the influent flow hydrodynamics on the membrane surface was researched. Fig. 5 and Fig. 6 show the velocity and pressure profiles on the membrane surface under three different operational conditions. The fluid flowed upward in the space between the channel and membrane. Fig. 5(a) presents a predicted velocity profiles on the membrane surface in five velocities, and Fig. 5(b) shows speed profiles at different sections.

3.2.1 Velocity profiles on the membrane surface under different operational conditions

The cross-flow velocity of the membrane surface was generally low at about 0.035 m/s while the inlet velocity was 0.23 m/s (Fig. 5). Nevertheless, the average cross-flow velocities reached 0.048 m/s and 0.066 m/s while the inlet velocities were 0.31m/ s and 0.40 m/s, respectively, and the high velocity near the central axis of membrane began to increase, the cross-flow velocity went down gradually along with the increased distance from the axis. The lower cross-flow velocity was difficult to guarantee the high stability of the FO permeate process, which is mainly because the lower inlet velocities in the system would lead to strong erosion of the entrance and weak erosion on both sides of membrane, and could not cover the entire membrane surface [52,53]. Therefore, it is necessary to set a suitably large inlet velocity during the FO process. The distribution area of the higher velocity was increasingly wide with the increase of inlet velocity. When the inlet velocity reached 0.55 m/s and 0.66 m/s, the average velocities of the membrane surface were 0.098 m/s and 0.12 m/s, respectively. Gruber et al. [54] used CFD simulation to study the influence of different cross-flow velocities on the change of water flux in the FO process and showed that by increasing the tangential flow rate along the FO channel, the external concentration polarization could be slowed down, and the membrane flux could be increased. In this study, the area of high fluid velocity could basically cover the entire membrane surface. The whole flow field was in a state of high cross-flow velocity, which could ensure preferable solute mixing and infiltration at each position of the membrane surface during the FO process.

Clearly, Fig. 5 shows that different inlet velocity caused the variation of membrane velocity and distribution, and the membrane cross-flow velocity increased with the increase of inlet velocity. A higher velocity was evident near the inlet entrance, and the velocities at

velocities of 0.23 m/s, 0.31m/s and 0.40m/s had a non-uniform distribution. The higher velocity concentrated at the center of the membrane along the longitudinal direction, while decreasing away from the center position. When the velocities were 0.55 m/s and 0.66 m/s, the higher velocity covered a larger proportion of the membrane surface than the lower did. Greater cross-flow velocity was at higher velocities on the membrane surface, while increasing the turbulence of feed solution, which accelerated the solute transfer from the membrane surface layer to the bulk solution, and relieved the negative effects caused by the ECP. This observation was proven in previous studies. For example, Elimelech and Phuntsho [55, 56] have shown that the increase of the flow velocity could increase the effective osmotic pressure difference to a certain extent and promote the permeability coefficient of water, which was beneficial to the permeation of pure water to the outside of the membrane. More importantly, it can effectively flush the membrane surface to avoid the accumulation of solute molecules and slow down the concentration polarization to ensure the continuous and stable infiltration process. The current study also revealed that the increased velocity improved the effective osmotic driven-force difference and subsequently enhanced the water permeation.

In conclusion, the results thus showed that (1) a spatial changing in velocity distribution was generated along the channel, and then the permeate flux changed, and (2) due to higher velocities, higher diffusion loads existed at specific locations on the membrane surface. Moreover, on account of the high velocity generated through flow scour, the diffusion load on a particular membrane may result in lower fouling.

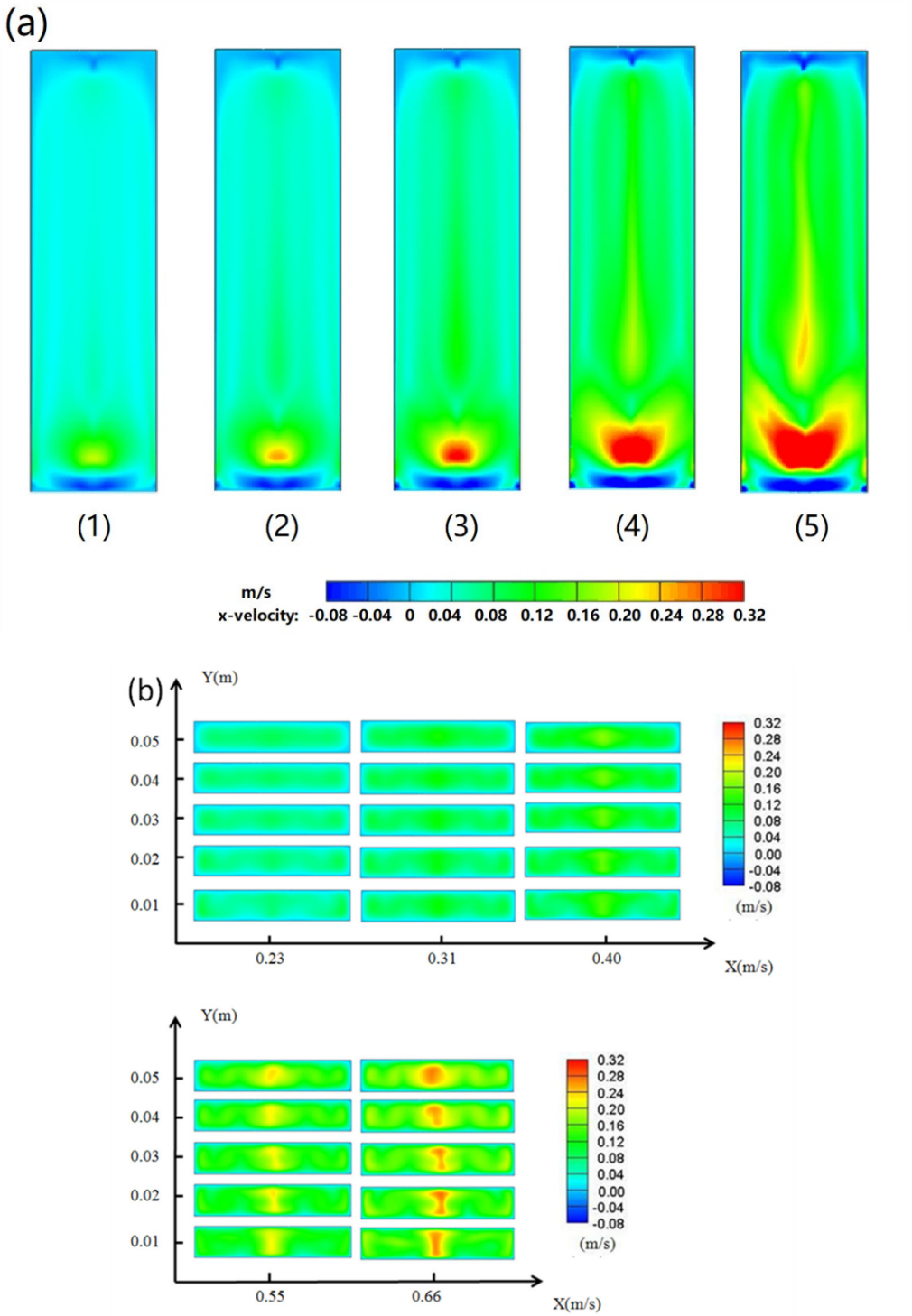

Fig. 5. The liquid velocity contour maps on the 7 cm × 2.5 cm membrane surface at various velocities: (a) velocity profiles on the membrane surface (b) speed profiles at different sections.

3.2.2 Pressure profiles on the membrane surface under different operational conditions

Fig. 6 illustrates the membrane pressure assignment under five velocities, which increased slightly in tandem with the velocities increased. The pressure distribution of the membrane

surface presents a basically uniform distribution at various velocities. When the inlet velocities were 0.23 m/s, 0.31 m/s and 0.40 m/s, the average pressures of the membrane surface were 80Pa, 120Pa and 180Pa, respectively, as shown in Fig. 6(a). The pressure on the membrane surface increased modestly with the inlet velocity increased. However, when the inlet velocity reached 0.55 m/s and 0.66 m/s in Fig. 6(b), the average pressure of the membrane surface increased to 300 Pa and 500 Pa, respectively. The membrane pressure assignment in these case was distinctly higher than in other cases. This result showed that the pressure assignment on the membrane surface varied with the change of inlet velocities. The pressure distribution over the overall membrane area was relatively uniform, except near the inlet location where the higher distribution of pressure was produced by hydraulic impact. This may be because with the increase of inlet velocity, the fluid particle had a movement tendency perpendicular to the membrane surface, which affected the infiltration process, in addition to the movement along the length of the membrane [57]. Furthermore, this movement tendency also promoted the penetration of water molecules. And the hydraulic pressure benefited the water permeation process and enhanced the mass transfer [58].

As a consequence, the higher membrane pressure produced by enhancing inlet velocity helped improve the permeability of the FO process. Velocities of 0.55m/s and 0.66m/s, which showed good permeability, were identified as better operating conditions in this FO process.

Therefore, these simulation results indicate that spatial changes in velocity and pressure distribution along the channel were followed by changes in permeate flux. Nevertheless, the pressure distribution in the whole membrane surface was relatively uniform. Furthermore, membrane surface performance could be optimized by increasing the inlet velocity, thereby enhancing the performance of the FO process. When the inlet velocities were 0.55m/s and

0.66m/s, the cross-flow velocity and pressure of the membrane surface were larger and the distribution was relatively uniform, which was electively better operating condition. However, there is also energy consumption for increasing the velocity to improve the flow field. Hence, taking into account both of the two factors, a velocity of 0.55 m/s should be selected as the operation state.

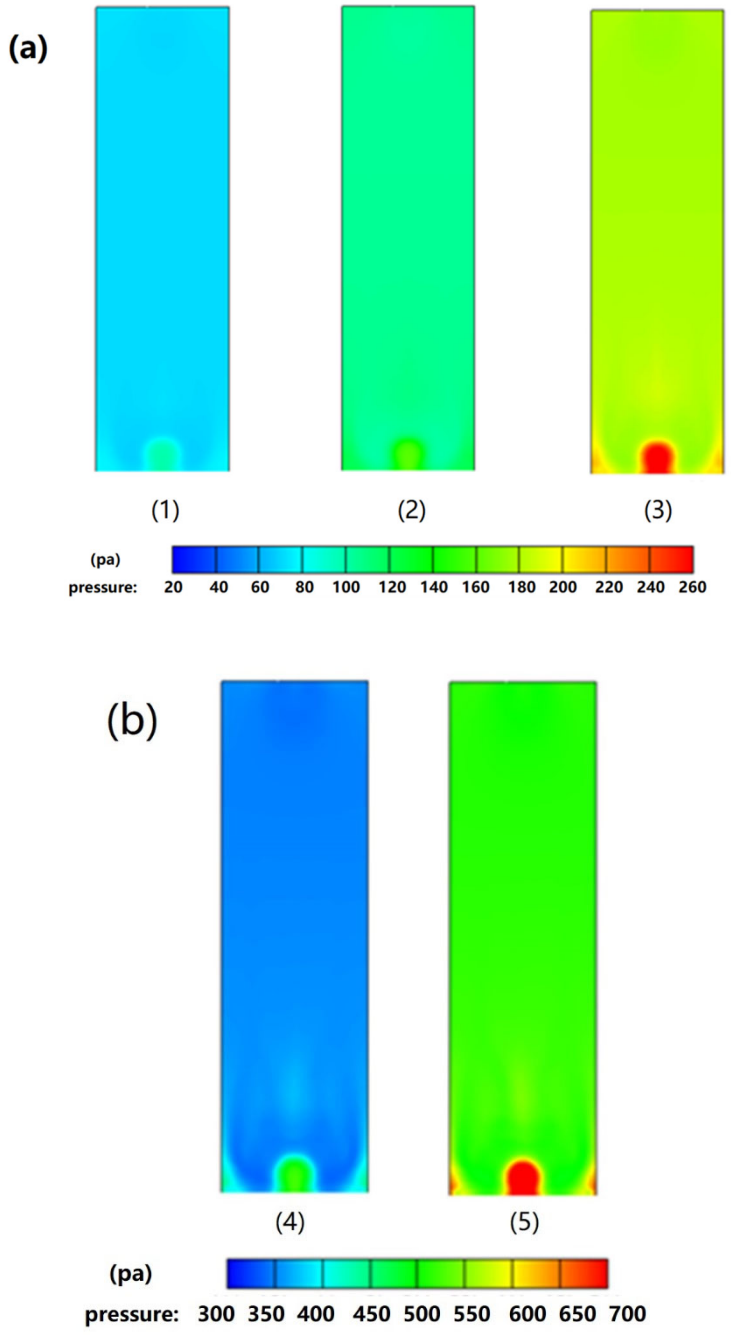

Fig. 6. The pressure distribution on the 7 cm × 2.5 cm membrane surface at various velocities:

(1) the inlet velocity is 0.23 m/s, (2) the inlet velocity is 0.31 m/s, (3) the inlet velocity is 0.40 m/s, (4) the inlet velocity is 0.55 m/s, (5) the inlet velocity is 0.66 m/s.

3.3. Impact of spacers' configuration

3.3.1 Impact of the number of spacers

The selection of the number of submerged-type spacers in this study, was taken into consideration the result of previous study that of all the configurations, submerged-type spacers performed the best [59]. The spacer diameter was 1 mm and the distance between the spacers was 2 mm in the numerical simulation. This section mainly presents the influence of the number of spacers on the flow field at the membrane surface. The velocity and the membrane surface pressures were simulated at the inlet velocity of 0.23 m/s when three spacer numbers (N=1, 11, 18) were added to the modules (Fig. 7, 8).

In Fig. 7, the value of pressure gradually increased with the increase of the spacer number. The values of pressure near the center region of the membrane in three spacers varying from 1 to 18 at the inlet velocity of 0.23 m/s were 63 Pa, 75 Pa, and 94 Pa. The pressure values of membrane were generally at a high level and mostly distributed in the area where the spacer was located, as the spacers were evenly distributed within the module. The fluid flow, barricaded slightly due to the presence of spacers, caused pressure changes on the membrane surface. The outcome of pressure change might be beneficial to mass transfer in the osmosis process. The velocity distribution on the membrane surface at three spacer numbers are illustrated in Fig. 8. When the spacer number was 1, the higher velocity was approximately 0.096 m/s, concentrated at the center of the membrane along the width direction, while the velocity on other positions was relatively low. This may be attributed to the presence of spacer resulting in restricted membrane fluid flow, which in turn caused the non-uniformity of the

velocities distribution on the membrane [60]. When N = 11, the spacers were distributed over most of the module. Obviously, the flow velocity in the area with no spacer began to decrease, and the inhomogeneity of the whole membrane surface still existed. When F or N = 18, the spacer had a complete coverage inside the module, and the distribution of the higher velocity region was wider, which is better than that in other cases.

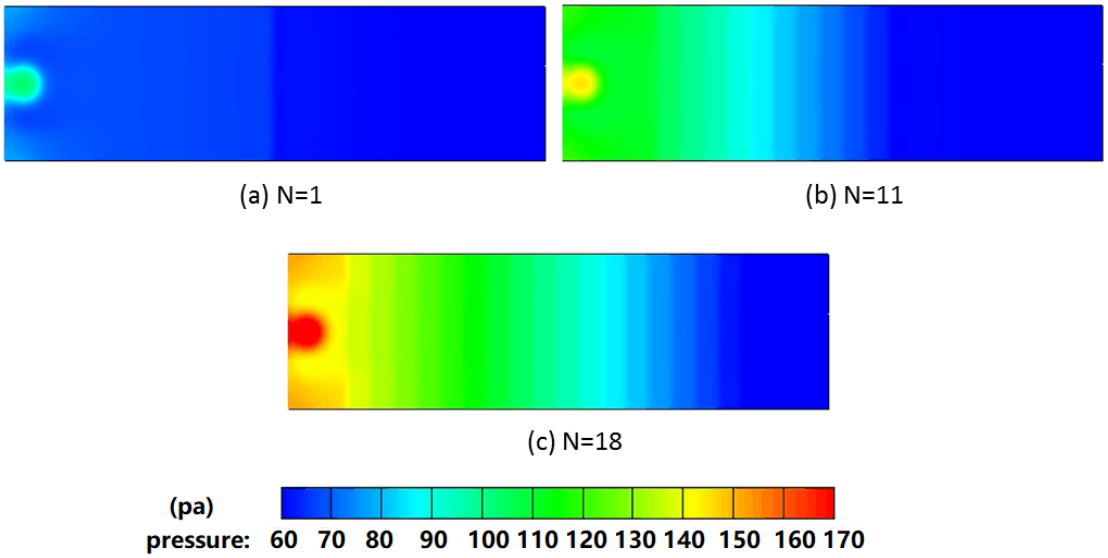

Fig. 7. The pressure distribution upon the membrane surface at different numbers: (a) N=1, (b) N=11, (c) N=18.

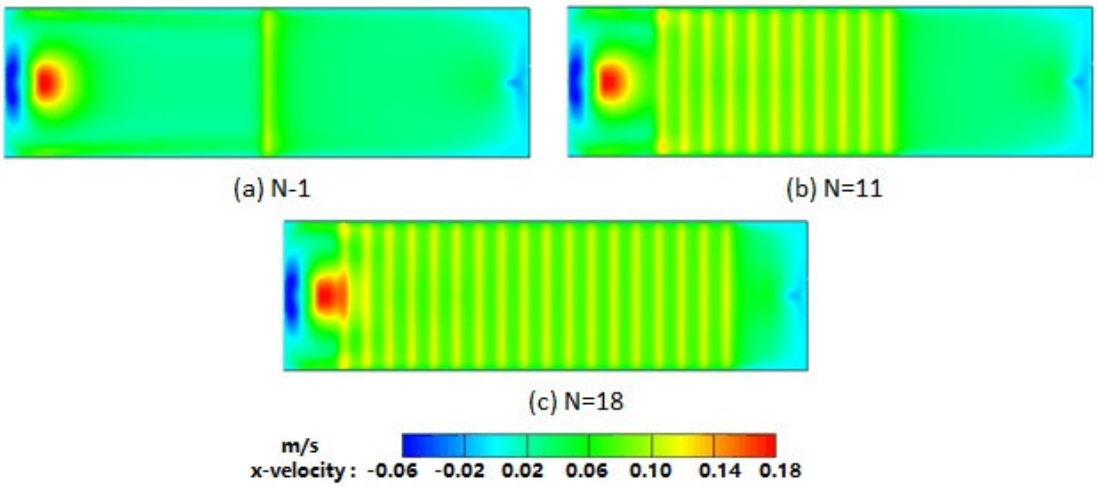

Fig. 8. The velocity contour upon the membrane surface at different numbers: (a) N=1, (b) N=11, (c) N=18.

In conclusion, the velocity and pressure on the membrane surface showed non-uniform

distribution due to the location of the spacers. The phenomenon of non-uniform distribution remained when the number was 11. Optimum velocity on the membrane surface occurred when the spacer number was 18, and at that particular moment, the spacers were evenly distributed in the channel. The presence of spacers ensured a more uniform spatial mass-transfer over the membrane and increased the average membrane mass-transfer in the osmosis process [53]. As a result, 18 spacers were selected as the ideal spacer configuration.

3.3.2 Impact of space structure

In the modules, three spacer positions (0.3 mm, 1 mm and 2 mm away from the membrane) between the membrane and channel were used to examine the hydrodynamics of fluid flow. And the spacers were guaranteed to be uniformly distributed. The liquid velocities of membrane surface were analyzed in the flowing sections at the channel width of 1 mm, upward along the length direction of the module.

Fig. 9 illustrates the velocity streamlines (the partially enlarged detail) of solution in the channels. When the spacer was 0.3 mm away from the membrane, the flow velocities in the FO feed channel demonstrated obvious variation in the transverse direction, accompanied with the emergence of vortex. However, the low fluid velocity over the membrane surface could generate the negative influence on mass transfer. On one hand, spacers could increase the cross flow on the membrane interface to some extent and lead to the greater turbulence in the channel. On the other hand, the spacer could infect the drag friction of boundary layer, which resulted in the loss of momentum and intensified degree of ECP [61]. When the spacer is 1mm away from the film, the average velocity is about 0.041 m/s, which is higher than the average velocity above the film when the spacer is 2 mm away from the film, which is 0.036 m/s. In the high velocity scenario, the particles in the FS were much easier to leave from the membrane surface

to the stream, which could alleviate ECP effectively.

To improve FO permeability, a higher cross-flow velocity would have a better effect on the penetration of water molecules and the shear force on the membrane surface [60]. Hence, considering FO flow conditions which have on the most favorable permeability, the optimum spacer configuration existed when the spacers were 1 mm away from the membrane.

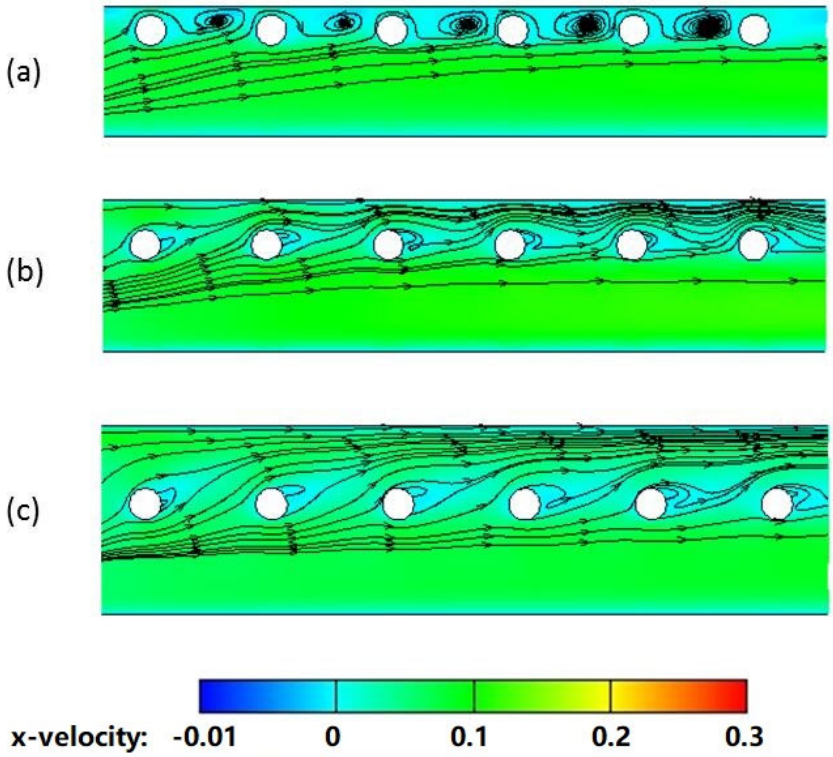

Fig. 9. The influence of different spacer positions on the streamlines of the membrane surface: (a) 0.3 mm away from membrane, (b) 1 mm away from membrane, and (c) 2 mm away from membrane.

3.4. Comparison of experiments and simulations

In this section, the pressure caused by the cross-flow was calculated based on Eq (2). The CFD simulation was confirmed by the lab experiment in which four different velocities were adopted ranging from 0.25 m/s to 0.40m/s at the module inlet. According to Fig. 10, the experiment and simulated results of the shear pressure on the surface were coincident. Furthermore, a good agreement between experimental and CFD results motivated further

numerical studies regarding the effects on the pressure and flow velocity distribution of changing cross-flow velocity. The results showed that piezo film could be used an effective sensor in the micro-hydraulic monitoring. Moreover, based on the stable chemical properties of piezo film sensor, the algae activity would not affect the piezo film sensor and thus it can be used for micro-hydraulic monitoring.

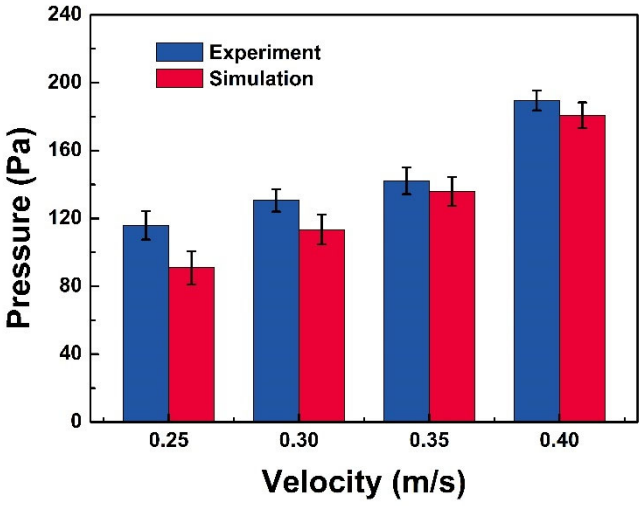

Fig. 10. The value of pressure upon the membrane surface under different velocities.

4. Conclusions

This study aimed to optimize the hydraulic character on FO membrane surface by analyzing the pressure and velocity distribution in microalgae dewatering process. Numerical simulation based on piezo film measuring method was combined with experimental investigation. We found that the pressure and the velocity distribution were affected by the flow rates at the module inlet and the spacer's configuration in the stable microalgae dewatering operation. The optimum spacer configuration was determined in this investigation. The results demonstrated that the velocity distribution was relatively uniform and exerted a higher pressure on the membrane when the velocity was 0.55 m/s. With reference to spacer configuration,

spacers were evenly distributed in the channel and the optimum spacer configuration existed when the spacers were 1 mm away from the membrane. At the same time, the CFD simulations were validated by experimental measurements with a reasonable margin for error. Therefore, better hydraulic conditions in microalgae dewatering determined the efficiency and productivity of the dewatering process. Further research is necessary on optimizing feed spacer, using FO to dewater other algae species and using different draw solutions.

Acknowledgements

This study was financially supported by the National Natural Science Foundation of China (No. 51978464, 51578375), China Postdoctoral Science Foundation (2017M621081), Tianjin Science and Technology Plan Project (No. 16PTGCCX00070). The research collaboration between Tianjin Polytechnic University and University of Technology Sydney is grateful.

References:

[1] Liliana Rodolfi，Graziella Chini Zittelli，Niccolò Bassi, Microalgae for oil: Strain selection, induction of lipid synthesis and outdoor mass cultivation in a low-cost photobioreactor, Biotechnology and Bioengineering. 102(2009)100-112.

[2] Pragya N, Pandey K K, Sahoo P K, A review on harvesting, oil extraction and biofuels production technologies from microalgae, Renewable & Sustainable Energy Reviews. 24(2013)159-171.

[3] M. Zhang, L. Yao, E. Maleki, B.Q. Liao, H. Lin, Membrane technologies for microalgal cultivation and dewatering: Recent progress and challenges, Algal Res. 44 (2019) 101686.

[4] Chung.T.S, Zhang. S, Wang.K.Y, Su.J.C, Ling.M.M, Forward osmosis processes:

yesterday, today and tomorrow. Desalination. 287 (2011) 78-81.

[5] Lutchmiah Kerusha, Cornelissen Emile R, Harmsen Danny J H, Post Jan W, Lampi Keith, Ramaekers Hans, Rietveld Luuk C, Roest Kees, Water recovery from sewage using forward osmosis. Water science and technology: a journal of the International Association on Water Pollution Research. 773 (2011) 1443-1449.

[6] C.Y.Chen, K.L.Yeh, R. Aisyah, D.J.Lee, J.S.Chang, Cultivation photobioreactor design and harvesting of microalgae for biodiesel production: a critical review, Bioresoure Technology. 102 (2011) 71-81.

[7] M. Rickman, J. Pellegrino, R. Davis, Fouling phenomena during membrane filtration of microalgae, J. Membrane. Science. 423 (2012) 33-42.

[8] Landels Andrew, Beacham Tracey A, Evans Christopher T, Carnovale Giorgia, Raikova Sofia, Cole Isobel S, Goddard Paul, Chuck Christopher, Allen Michael J, Improving electrocoagulation floatation for harvesting microalgae, Algal Research-Biomass Biofuels and Bioproducts. 39 (2019) 101446.

[9] Yusra Shahid, Raja Ghosh, Dewatering of microalgae suspension using air-sparged ultrafiltration, Separation Science and Technology. (2017) 344-351.

[10] Yi Zheng, Wenxiang Zhang, Bing Tang, Jie Ding, Yi Zheng, Zhien Zhang, Membrane fouling mechanism of biofilm-membrane bioreactor (BF-MBR): Pore blocking model and membrane cleaning, Bioresource Technology. 036 (2018) 398-405.

[11] Cath. T, Childress. A, Elimelech. M, Forward osmosis: Principles, applications, and recent developments, Journal of Membrane Science. 281 (2006) 70-87.

[12] Shaffer.D.L, Werber.J.R, Jaramillo. H, Forward osmosis: Where are we now? Desalination. 356 (2015) 271–284.

[13] Zhao. S, Zou. L, Tang.C.Y, Mulcahy. D, Recent developments in forward osmosis: opportunities and challenges, J. Membr. Sci. 396 (2012) 1–21.

[14] W. Xu, Q. Zhen, Q. Ge, Recent advances in forward osmosis (FO) membrane: chemical modifications on membranes for FO processes, Desalination. 419 (2017) 101–116.

[15] D. Li, Y. Yan, H. Wang, Recent advances in polymer and polymer composite membranes for reverse and forward osmosis processes, Prog. Polym. Sci. 61 (2016) 104–155.

[16] B. Mi, M. Elimelech, Organic fouling of forward osmosis membranes: fouling reversibility and cleaning without chemical reagents, J. Membr. Sci. 348 (2010) 337–345.

[17] C. H, Tan.H, Y.Ng, Modified models to predict flux behavior in forward Osmosis in consideration of external and internal concentration polarizations, J. Membr. Sci. 324 (2008) 209-219.

[18] Suh. C, Lee. S, Modeling reverse draw solute flux in forward osmosis with external concentration polarization in both sides of the draw and feed solution, Journal of Membrane Science.427 (2013) 365-374.

[19] Heikkinen. J, Kyllonen. H, Jarvela. E, Ultrasound-assisted forward osmosis for mitigating internal concentration polarization, Journal of Membrane Science. 528 (2017) 147-154.

[20] Wang.Y.F, Wang. J, Zhang.H.W, Wu. Y, Dang.A.H, Numerical and experimental investigation to determine the optimal configuration of an aeration component in the hollow fiber membrane cleaning process, Rsc Advantages. 26 (2016) 21600-21611.

[21] Zhang. H, Cheng. S, Yang. F, Use of a spacer to mitigate concentration polarization during forward osmosis process, Desalination. 307 (2014) 112-119.

[22] Elimelech. M, Phillip.W.A, The future of seawater desalination: energy, technology, and the environment, Science. 333 (2011) 712–717.

[23] Phuntsho. S, Sahebi. S, Majeed. T, Assessing the major factors affecting the performances of forward osmosis and its implications on the desalination process, Chem. Eng. J. 231 (2013) 484–496.

[24] Shibuy. M, Yasukaw. M, Goda. S, Experimental and theoretical study of a forward osmosis hollow fiber membrane module with a cross-wound configuration, Journal of Membrane Science. 504 (2016) 10-19.

[25] Du. X, Wang. Y, Qu.F.S, Impact of bubbly flow in feed channel of forward osmosis for wastewater treatment: Flux performance and biofouling, Chemical Engineering Journal. 316 (2017) 1047–1058.

[26] Hawari.A.H, Kamal. N, Altaee. A, Combined influence of temperature and flow rate of feeds on the performance of forward osmosis, Desalination. 398 (2016) 98–105.

[27] Lay. W, C.L, Zhang.J.S, TangFactors.C.Y, Factors effecting flux performance of forward osmosis systems, Journal of Membrane Science. 394 (2012) 151–168.

[28] Liu. P, Zhang. H, Feng. Y, Influence of spacer on rejection of trace antibiotics in wastewater during forward osmosis process, Desalination. 371 (2015) 134–143.

[29] Fimbres-Weihs.G.A, Wiley.D.E, Review of 3D CFD modeling of flow and mass transfer in narrow spacer-filled channels in membrane modules, Chemical Engineering and Processing. 49 (2010) 759–781.

[30] Gruber.M.F, Johnson.C.J, Tang.C.Y, Computational fluid dynamics simulations of flow and concentration polarization in forward osmosis membrane systems, Journal of Membrane Science. 379 (2011) 488–495.

[31] Rahimi. M, Madaeni.S.S, Abbasi. K, CFD modeling of permeate flux in cross-flow microfiltration membrane, Journal of Membrane Science. 255 (2005) 23–31.

[32] Gruber.M.F, Aslak. U, Helix-Nielsen. C, Open-source CFD model for optimization of forward osmosis and reverse osmosis membrane modules, Separation and Purification Technology. 158 (2016) 183–192.

[33] Wasilewski. J, Mirota. K, Peryt-Stawiarska. S, Nowakowski. A, Polonski. L, Zembala, M, An introduction to computational fluid dynamics based on numerical simulation of pulsatile flow in the left coronary artery, Polish Journal of Cardio-Thoracic Surgery. 3 (2012) 366–374.

[34] Hansen. M, Barker.V.A, Hassager. O, Spectral element simulation of ultrafiltration, Chem Eng Sci. 53 (1998) 3099–3115.

[35] Li. F, Meindersma. W, Haan.A.B, Optimization of commercial net spacers in spiral wound membrane modules, J Membr Sci. 208 (2002) 289–302.

[36] Wardeh. S, Morvan.H.P, CFD simulations of flow and concentration polarization in spacer-filled channels for application to water desalination, Chemical Engineering Research and Design. 86 (2008) 1107–1116.

[37] Cao.Z, Wiley.D.E, Fane.A.G, CFD simulation of net-type turbulence promoters in a narrow channel, Journal of Membrane Science. 185 (2001) 157–176.

[38] Abdelbadie. M, El-Refaee. M, A 3D CFD comparative study between torsioned and non-torsioned net-type feed spacer in reverse osmosis, SN Applied sciences. 1(2019) 9.

[39] Shakaib. M, Hasani. S, M. F, Mahmood. M, CFD modeling for flow and mass transfer in spacer-obstructed membrane feed channels, Journal of Membrane Science. 326 (2009) 270-284.

[40] Jung.D.H, Lee. J, Kim.D.Y, Simulation of forward osmosis membrane process: Effect of membrane orientation and flow direction of feed and draw solutions, Desalination. 377

(2011) 83–91.

[41] Takashi Hibiki, Joshua P. Schlegel, Tetsuhiro Ozaki, Shuichiro Miwa, Somboon Rassame, Simplified two-group two-fluid model for three-dimensional two-phase flow Computational Fluid Dynamics for vertical upward flow, Progress in Nuclear Energy.108 (2017) 503-516.

[42] Y.Y. Liang, K.Y. Toh, G.A. Fimbres Weihs, 3D CFD study of the effect of multi-layer spacers on membrane performance under steady flow, Journal of Membrane Science. 580 (2019) 256-267.

[43] Gassan Hodaifa, Sebastián Sánchez, Mª. Eugenia Martínez, Rafael Órpez, Biomass production of Scenedesmus obliquus from mixtures of urban and olive-oil mill wastewaters used as culture medium, Appl. Energy. 104 (2013) 345–352.

[44] Satu. R, Jukka. L, PVDF and EMFi sensor materials - A comparative study, Procedia Engineering. 5 (2010) 862–865.

[45] Saketi.P, Latifi.S.K, Hirvonen. J, PVDF microforce sensor for the measurement of Z-directional strengthZ- in paper fiber bonds, Sensors and Actuators Physical. 222 (2015) 194–203.

[46] Wang. Y, Brannock. M, Leslie. G, CFD simulations of membrane filtration zone in a submerged hollow fiber membrane bioreactor using a porous media approach, Journal of Membrane Science. 363 (2010) 57-66.

[47] Amini. E, Mehrnia.M. R, Mousavi.S.M, Experimental Study and Computational Fluid Dynamics Simulation of a Full-Scale Membrane Bioreactor for Municipal Wastewater Treatment Application, Industrial & Engineering Chemistry Research.52(2013) 9930−9939.

[48] Park. M, Kim.J.H, Numerical analysis of spacer impacts on forward osmosis membrane process using concentration polarization index, Journal of Membrane Science. 427 (2013) 10–20.

[49] Wang.Y, Zhang.M.K, Liu.Y.Q, Xiao.Q.Q, Xu.S.C, Quantitative evaluation of concentration polarization under different operating conditions for forward osmosis process, Desalination. 398 (2016) 106–113.

[50] Yip. Y, Tiraferri. A, Phillip. A, Schiffman. D, Elimelech. M, High performance thin-film composite forward osmosis membrane. Environmental scienence & Technology, 44(2010) 3812-8.

[51] Munshi.M, Church.J, Mclean.R, Dewatering algae using an aquaporin-based polyethersulfone forward osmosis membrane. Separation and Purification Technology, 204(2018)154-161.

[52] Akther. N , Daer. S , Wei. Q, Synthesis of polybenzimidazole (PBI) forward osmosis (FO) membrane and computational fluid dynamics (CFD) modeling of concentration gradient across membrane surface, Desalination. 452(2019)17-28.

[53] Qing. L, Bilad. R, Sun. G, Flow uneven-distribution and its impact on performances of forward osmosis module, Journal of Water Process Engineering. 33 (2020) 101014.

[54] Gruber.M.F, Johnson.C.J, Tang. C, Jensen.M.H, Validation and Anlysis of Forward Osmosis CFD Model in Complex 3D Geometries, Membranes. 2 (2012) 764-782.

[55] Elimelech. M, Phillip. A, The future of seawater desalination: energy, technology, and the environment, Science. 333(2011)712–717.

[56] Phuntsho. S, Sahebi. S, Majeed. T, Assessing the major factors affecting the performances of forward osmosis and its implications on the desalination process, Chemical Engineering

Journal. 231(2013)484–496.

[57] Xiao Mao. Wang, XY. Li, Modeling of the initial deposition of individual particles during the cross-flow membrane filtration, Colloids & Surfaces A Physicochemical & Engineering Aspects. 440(2014)91-100.

[58] Weichen. Lin, Ruipeng. Shao, Xiaomao. Wang, Xia. Huang, Impacts of non-uniform filament feed spacers characteristics on the hydraulic and anti-fouling performances in the spacer-filled membrane channels: Experiment and numerical simulation, Water Research. 185 (2020) 116251.

[59] Fang Xie, Weiwei Chen, Jianmin Wang, Jinrong Liu, CFD and experimental studies on the hydrodynamic performance of submerged flat-sheet membrane bioreactor equipped with micro-channel turbulence promoters, Chemical Engineering and Processing: Process Intensification. 99 (2016) 72-79.

[60] Ahmed M. Alshwairekh, Abdullah A. Alghafifis, Anas M. Alwatban, Umar F. Alqsair, Alparslan Oztekin, The effects of membrane and channel corrugations in forward osmosis membrane modules–Numerical analyses, Desalination. 460 (2019) 41–55.

[61] Mathieu Larronde-Larretche, Xue Jin, Microalgae (Scenedesmus obliquus) dewatering using forward osmosis membrane: Influence of draw solution chemistry, Algal Research. 15(2016)1-8.